Astronomy & Astrophysics manuscript no. blf
June 11, 2010

LETTER TO THE EDITOR

CHESS: Chemical Herschel surveys of star forming regions : Peering into the protostellar shock L1157-B1. ⋆

II. Shock dynamics

Lefloch B.[1], Cabrit S.[2], Codella C.[3], Melnick G.[4], Cernicharo J.[5], Caux E.[6], Benedettini M.[7], Boogert A.[8], Caselli P.[9], Ceccarelli C.[1], Gueth F.[10], Hily-Blant P.[1], Lorenzani A.[3], Neufeld D.[11], Nisini B.[12], Pacheco S.[1], Pagani L.[2], Pardo J.R.[5], Parise B.[13], Salez M.[2], Schuster K.[10], Viti S.[12,14], Bacmann A.[1,15], Baudry A.[15], Bell T.[16], Bergin E.A.[17] Blake G.[16], Bottinelli S.[6], Castets A.[1], Comito C.[13], Coutens A.[6], Crimier N.[1,5], Dominik C.[18,29], Demyk K.[6], Encrenaz P.[2], Falgarone E.[2], Fuente A.[20], Gerin M.[2], Goldsmith P.[21], Helmich F.[22], Hennebelle P.[2], Henning T.[23], Herbst E.[24], Jacq T.[15], Kahane C.[1], Kama M.[18], Klotz A.[6], Langer W.[21], Lis D.[16], Lord S.[16], Maret S.[1], Pearson J.[21], Phillips T.[16], Saraceno P.[7], Schilke P.[13,25], Tielens A.G.G.M.[26], van der Tak F.[22,19], van der Wiel M.[19,22], Vastel C.[6], Wakelam V.[15], Walters A.[6], Wyrowski F.[13], Yorke H.[21], Bachiller R.[20], Borys C.[16], De Lange G.[22], Delorme Y.[5], Kramer C.[25,27], Larsson B.[28], Lai R.[30], Maiwald F.W.[21], Martin-Pintado J.[5], Mehdi I.[21], Ossenkopf V.[25], Siegel P.[21], Stutzki J.[25], and Wunsch J.H.[13]

(Affiliations can be found after the references)

2010 March 31; 2010 April 30

ABSTRACT

Context. The outflow driven by the low-mass class 0 protostar L1157 is the prototype of the so-called chemically active outflows. The bright bowshock B1 in the southern outflow lobe is a privileged testbed of magneto-hydrodynamical (MHD) shock models, for which dynamical and chemical processes are strongly interdependent.

Aims. We present the first results of the unbiased spectral survey of the L1157-B1 bowshock, obtained in the framework of the key program "Chemical Herschel Surveys of Star Forming Regions" (CHESS). The main aim is to trace the warm and chemically enriched gas and to infer the excitation conditions in the shock region.

Methods. The CO 5-4 and o-H_2O $1_{10} - 1_{01}$ lines have been detected at high-spectral resolution in the unbiased spectral survey of the HIFI-Band 1b spectral window (555-636 GHz), presented by Codella et al. in this volume. Complementary ground-based observations in the submm window help establish the origin of the emission detected in the main-beam of HIFI, and the physical conditions in the shock.

Results. Both lines exhibit broad wings, which extend to velocities much higher than reported up to now. We find that the molecular emission arises from two regions with distinct physical conditions : an extended, warm (100 K), dense (3×10^5 cm^{-3}) component at low-velocity, which dominates the water line flux in Band 1; a secondary component in a small region of B1 (a few arcsec) associated with high-velocity, hot (> 400 K) gas of moderate density ($(1.0 - 3.0) \times 10^4$ cm^{-3}), which appears to dominate the flux of the water line at 179 μm observed with PACS. The water abundance is enhanced by two orders of magnitude between the low- and the high-velocity component, from 8×10^{-7} up to 8×10^{-5}. The properties of the high-velocity component agree well with the predictions of steady-state C-shock models.

Key words. ISM: individual objects: L1157 — ISM: molecules — stars: formation

1. Introduction

Shocks in protostellar outflows play a crucial role in the molecular cloud evolution and star formation by transferring momentum and energy back to the ambient medium. There is mounting evidence that these shocks often involve a magnetic precursor where ionic and neutral species are kinematically decoupled. Magneto-hydrodynamical (MHD) shocks are important not only for the cloud dynamics, but also for the chemical evolution through temperature and density changes, which favors the activation of endothermic reactions, ionization, and dust destruction through sputtering and shattering in the ion neutral drift zone. These various processes lead to abundance enhancements up to several orders of magnitude, as reported for various molecular species in "chemically active" outflows (Bachiller et al. 2001). Conversely, the magnetic field and the ionization fraction play an important role in controlling the size and the temperature of the ion-neutral drift zone. Because of the interplay between the dynamics and chemistry, the physics of MHD shocks requires a comprehensive picture of both the gas and dust physical conditions in the compressed region itself.

Along with H_2, H_2O and CO are two key-molecules predicted to dominate the cooling of MHD shocks (Kaufman & Neufeld 1996). The abundance of H_2O in protostellar regions can be greatly enhanced in shocks, even of moderate velocity. This occurs both from the sputtering of frozen water from grain mantles and through high-temperature sensitive reactions in the gas phase (Elitzur & de Jong, 1978; Elitzur & Watson, 1978; Bergin et al. 1998). Multi-transition observations of these two

⋆ *Herschel* is an ESA space observatory with science instruments provided by European-led Principal Investigator consortia and with important participation from NASA.

molecules therefore serve as good probes of shock regions with various excitation conditions, and can be used to set stringent constraints on MHD shock models (Flower & Pineau des Forets, 2010).

The heterodyne instrument HIFI onboard *Herschel* allows us to study with unprecedented sensitivity the chemical and dynamical evolution of protostellar shocks, at spectral and angular resolutions comparable to the best ground-based single-dish telescopes. This is the main goal of the spectral survey of L1157-B1, carried out in the guaranteed time key-project CHESS.

The source L1157-mm is a low-mass Class 0 protostar located at a distance estimated between 250 pc (Looney et al. 1997) and 440 pc (Viotti 1969). It drives a spectacular bipolar outflow, which has been studied in detail at millimeter and far-infrared wavelengths. Mapping of the southern lobe of L1157 with the Plateau de Bure Interferometer (PdBI) reveals two limb-brightened cavities (Gueth et al. 1996), each one terminated by a strong bow shock, dubbed "B1" and "B2" respectively (Fig. 1), which are likely the result of episodic ejection events in a precessing, highly collimated jet. The spatial and kinematical structure of B1 has been modelled in great detail by various authors, making it the archetype of protostellar bowshocks in low-mass star-forming regions and the testbed of MHD shock models (Gusdorf et al. 2008a,b).

Here, we report on the emission lines of CO and H_2O detected in the low-frequency band of HIFI in the course of the CHESS spectral survey. From comparison with complementary observations, we discuss the origin of the emission, and based on a simple modelling of the source, we derive the water abundance in the shock region.

2. Observations and results

A full coverage of the band 1b at $20^h39^m10.2^s$ +68°01′10.5″ (J2000) in the bowshock B1 was carried out with the HIFI heterodyne instrument (de Graauw et al. 2010) on board of the *Herschel* Space Observatory (Pilbratt et al. 2010) during the Performance Verification phase on 2009 August 1. The corresponding dataset is OBS_1342181160. The HIFI band 1b (from 555.4 to 636.2 GHz) was covered in double beam switching. Both polarizations (H and V) were observed simultaneously. The receiver was tuned in double sideband (DSB) with a total integration time of 140 minutes. In order to obtain the best possible data reconstruction, the survey was acquired with a degree of redundancy of 4. The Wide Band Spectrometer (WBS) was used as spectrometer, providing a frequency resolution of 0.5 MHz.

The data were processed with the ESA-supported package HIPE (Ott et al. 2009). Fits file from level 2 were then created and transformed into GILDAS format[1] for baseline subtraction and subsequent sideband deconvolution. The spectral resolution was degraded to 1MHz in the final single sideband (SSB) dataset. The calibration for each receiver (H and V) is better than 2-3%. The relative calibration between both receivers is also rather good, with a difference in intensity of about 4%. The overall calibration uncertainty is about 7%, except for the strong CO line present in the band (see below).

Two strong lines dominate over the molecular transitions detected in the spectral band: the fundamental line of water in its ortho state o-H_2O $1_{10} - 1_{01}$ at 556.936069 GHz and the CO 5-4 line at 576.276905 GHz (Fig. 1). The final rms noise is 13 mK. We adopted the theoretical telescope main-beam efficiency $\eta_{mb} = 0.723$, and a main-beam size of 39″ (HPFW) in the whole band. Unless indicated, intensities are expressed in units of antenna temperature T_A.

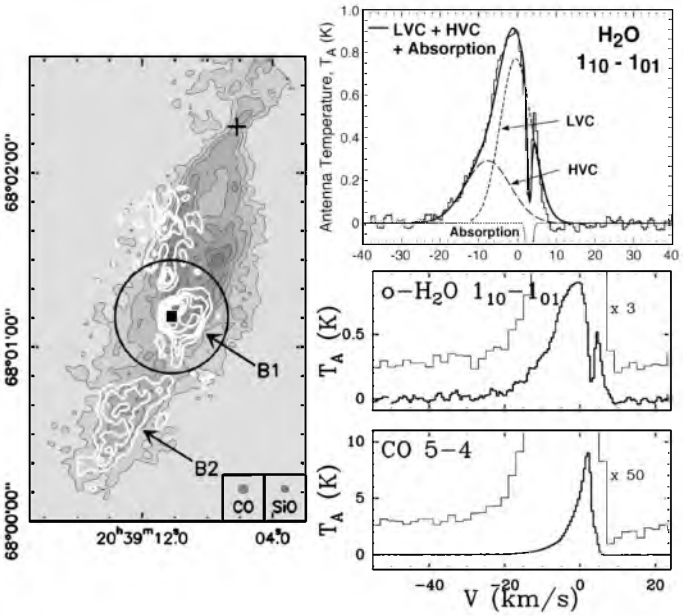

Fig. 1. *(left)* Southern outflow lobe of L1157 in CO 1-0 (greyscale and black contours) and in SiO 2-1 (white contours) as observed at the PdBI (Gueth et al. 1996,98). A black square marks the nominal position of bowshock L1157-B1 observed with HIFI. The HIFI main-beam is represented with a black circle. *(right)* Panel of the CO 5-4 (bottom) and o-H_2O $1_{10} - 1_{01}$ (centre) line spectra obtained in band 1b of HIFI. For both lines, we show (dashed) a magnified and spectrally smoothed view of the emission. Intensities are expressed in units of antenna temperature.(*top*) H_2O spectrum with fitted low-velocity component (LVC), high-velocity component (HVC), absorption feature and summed fitted spectrum.

The CO 5-4 transition is detected with an intensity of 9 K (T_A) and a linewidth of 5 km s^{-1}. We notice a weak absorption feature in the line profile in the redshifted gas over a wide velocity range, which may partly arise from cloud contamination in the reference position. The intensity in the blue wing of the CO line differs by as much as 20% between both polarizations. This effect is not observed towards the H_2O line. Its origin is not understood at the moment.

The fundamental o-H_2O $1_{10} - 1_{01}$ line is detected with an intensity of 0.9 K (T_A) at the peak. It is characterized by a broad linewidth $\approx$ 15 km s^{-1}. The line displays an absorption dip at v_{lsr} = +2.9 km s^{-1} and a broad redshifted wing extending up to +8 km s^{-1}. The broad linewidth of the H_2O spectrum could be fit with three Gaussian velocity components, a low-velocity, a high-velocity, and an absorption component. The low (high) velocity component peaks at v_{lsr} = −0.58 km s^{-1} (−7.86 km s^{-1}); the linewidth and peak intensity derived from the fit are 9.56 km s^{-1} and 0.77 K (13.72 km s^{-1} and 0.29 K), respectively. The absorption component was fit by a narrow line Gaussian (ΔV = 1.38 km s^{-1}) of amplitude −0.48 K centered at v_{lsr} = +2.9 km s^{-1}. The fit of the individual components and the resulting fit to the water spectrum is displayed in Fig. 1.

Overall, the H_2O and CO emission are detected in the same velocity range. The high sensitivity of the HIFI observations permits the detection of emission from the entrained gas up to v_{lsr} = −30 km s^{-1}, i.e. about 10 km s^{-1} higher than was previously known from ground based observations. However, line

[1] http://www.iram.fr/IRAMFR/GILDAS

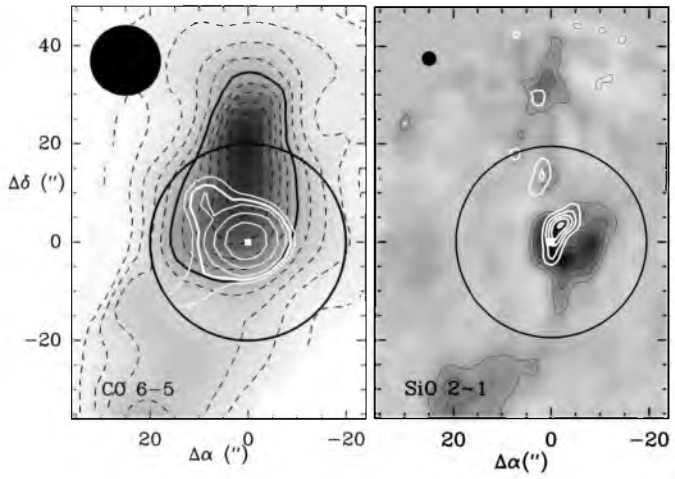

Fig. 2. *(left)* Velocity-integrated CO 6-5 emission maps of the low- and high-velocity components. LVC (HVC) emission is represented in greyscale and thin dashed contours (white contours); first contour and contour interval are 3σ and 1σ (10% of the peak flux), respectively, Contours at half-power are drawn in thick. *(right)* Same for SiO 2-1 observed at the PdbI. The HIFI main-beam is represented with a black circle.

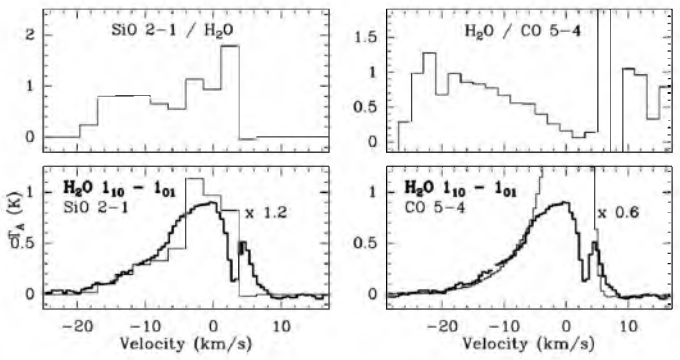

Fig. 3. (*bottom left*) Comparison of the o-H_2O $1_{10} - 1_{01}$ line profile with the SiO 2-1 emission observed at the PdBI, averaged over the HIFI beam. (*top left*) Variations of the SiO 2-1 / H_2O line ratio as a function of velocity. *(bottom right)* Comparison of the o-H_2O $1_{10} - 1_{01}$ and CO 5-4 line profiles. *(top right)* Variations of the H_2O /CO 5-4 line ratio as a function of velocity, smoothed to a resolution of 2 km s^{-1}.

profiles differ noticeably and the ratio of the H_2O/CO5 – 4 line intensities increases with increasing velocities from about 0.2 in the ambient gas up to 0.9 at $v_{lsr} = -25$ km s^{-1} (Fig. 3).

All the other molecular tracers detected in the HIFI band show a pronounced break in the line profile at $v_{lsr} \approx -7.2$ km s^{-1} (Codella et al. this volume). This is also observed in the CO 6-5 spectrum of B1 obtained by us at the CSO, as part of complementary observations to help analyse the CHESS data. The maps of the whole southern lobe of L1157 in CO 3-2 and 6-5 obtained at the CSO in June 2009, with 24″ and 14.5″ respectively, will be discussed in detail in a forthcoming paper (Lefloch et al. 2010, in prep.).

Below, we define the region with $v_{lsr} < -7.25$ km s^{-1} as the high-velocity component, hereafter HVC (see also Codella et al), and the region with $v_{lsr} > -7.25$ km s^{-1}) as the low-velocity component (LVC). As we discuss below, these two velocity components are characterized by different spatial extents and excitation conditions.

3. Discussion

3.1. Origin of the emission

Due to its relatively high energy above the ground state (E_{up} = 116 K) the CO 6-5 transition is a good probe of the warm regions where H_2O can evaporate from grain mantles and be released in the gas phase. SiO 2-1, observed at the PdBI at 2.5″ resolution is a particularly good tracer of shocks strong enough to release refractory elements in the gas phase, because it is usually undetected in the cold, quiescent molecular gas.

The overall SiO emission is strongly peaked at the position of B1, which appears as a region of ≈ 15″ size located at the apex of the cavity. Interferometric maps of the southern lobe (Figs. 1-2) reveal extended emission along the eastern wall of the cavity (the low-velocity wing of the bow) and downstream of B1, at velocities close to systemic, both blue and red. By comparing these data with IRAM 30m observations (Bachiller et al. 2001), we checked that unlike the HVC, a fraction of the flux emitted in the LVC is actually missed in the PdBI data, which is direct evidence for extended emission. This is consistent with the CO 6-5 data (Fig. 2). The low-velocity gas emission is located in the wake of B1, reaching ~ 40″ North from the apex. The area of the LVC amounts to ≈ 1/3 of the HIFI beam (see Fig. 2). Interestingly, the PACS map of the H_2O 179 μm line reveals large-scale emission, spatially coinciding with SiO 2-1 emission in the outflow (Nisini et al. 2010).

In any case, there is definitely much less molecular gas emission associated with the western wall of the cavity (Benedettini et al. 2007). We therefore expect an asymmetry in the H_2O spatial distribution, similar to that observed in many other tracers such as CS or HCN, as shown by the PACS map of the 179 μm H_2O line (Nisini et al. 2010).

We note an excellent agreement between the H_2O and the low-excitation SiO 2-1 line profiles (Fig. 3) in the high-velocity range, with a constant SiO 2-1 / H_2O line ratio ≈ 0.8 between -20 and −7 km s^{-1}. This has important implications. First, this constant ratio in the range of the HVC suggests that both emissions most likely arise from the same region and that the emissions are optically thick. In that case, the low intensities measured in the high-velocity component (a few tenths of K) point to a small size extent. This is direct evidence that the H_2O emission detected fills only partly the HIFI beam. Indeed, the bulk of the SiO HVC originates from a small region of 4″ × 12″ in B1 (Fig. 2), corresponding to a filling factor ff ~ 0.03 in the HIFI main-beam. Second, if silicon comes from grain erosion, the SiO profile is predicted to be much narrower than H_2O because it takes a long time for Si to oxidize into SiO, so SiO comes only from the cold postshock, as discussed by Gusdorf et al. (2008b). The similarity of the SiO and H_2O line profiles suggests that SiO forms more extensively in the shock than predicted by oxidation of sputtered Si atoms. As it can be released in the gas phase even at low velocities in the shock, SiO is present in the gas phase over the full width of the shock wave.

In summary, we find strong observational evidence that the emission from the HVC and LVC arises from regions of different physical extent. The size of the HVC appears definitely much lower than the LVC ($ff \simeq 0.03$ and 0.3, respectively). It is true however that the present determinations are uncertain. HIFI observations of the high-excitation lines of CO and H_2O will make

Table 1. Observed and fitted parameters of the H_2O and CO 5-4 lines and prediction for the 179 μm H_2O line flux. The CO fluxes in the HVC and LVC are integrated in the velocity intervals [-30;-7.25] and [-7.25; +11.0], respectively. The H_2O fluxes are derived from a multiple Gaussian fit to the line profile. Intensities are expressed in units of antenna temperature (T_A) K km s^{-1}.

	H_2O 557GHz (K km s^{-1})	CO 5-4 (K km s^{-1})	CO 6-5[1] (K km s^{-1})	CO 3-2[1] K km s^{-1}	Size ($''$)	N(CO)[2] (cm^{-2})	n(H_2)[2] (cm^{-3})	T[2] (K)	X(H_2O)[3] (cm^{-2})	F(179 μm) (W cm^{-2})
LVC	7.83	45.4	29.2	40.4	25	8.0(16)	(1.0-3.0)(5)	100	0.8(-6)	4.2(-20)
HVC	4.28	3.98	1.34	3.11	7	5.0(16)	(1.0-3.0)(4)	400	0.8(-4)	7.1(-20)

[1] From CSO observations smoothed down to the resolution of the HIFI observations.
[2] Determined from LVG analysis of the CO emission.
[3] From comparison of LVG-derived N(o – H_2O) with N(CO), assuming a water OPR of 3 and an abundance [CO]/[H_2] = 10^{-4}.

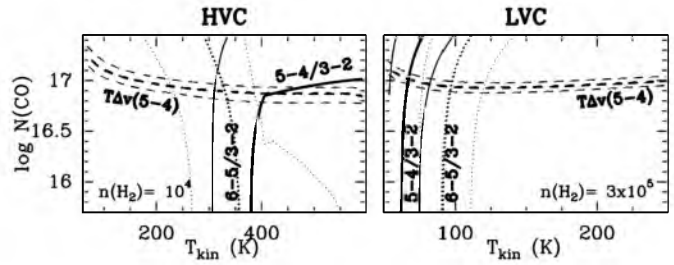

Fig. 4. Best-fit solution to the LVG modelling of CO line temperatures in the 3-2, 5-4 and 6-5 transitions for both HVC (left) and LVC (right) components, respectively. The contour of the observed CO 5-4 integrated line area (TΔv), corrected for main-beam dilution, is drawn in a dashed line, as well as the 5-4/3-2 and 6-5/3-2 line ratios (solid and dotted lines, respectively). Thin lines delineate the uncertainties in the observed values.

it possible to better establish appropriate filling factors for these components.

3.2. Physical conditions

We first estimated the physical conditions from the emission detected in the CO 3-2, 5-4, and 6-5 transitions both in HVC and LVC . We modelled each velocity component as a simple uniform slab, adopting the size (filling factor) estimated above. Calculations were done in the large-velocity gradient approach, using the CO collisional coefficients determined by Flower (2001) for ortho-H_2 collisions in the range 5 K-400 K. For temperatures beyond 400 K, the collisional coefficients were extrapolated adopting a temperature dependence of $\sqrt{T/400\,\mathrm{K}}$. Both components appear to have the same gas column density N(CO) $\simeq 10^{17}$ cm^{-2} (Fig. 4). We found the high-velocity gas component to be unambiguously associated with hot gas ($T > 350$ K) of moderate density $\approx 3.0 \times 10^4$ cm^{-3}, whereas the low-velocity component arises from gas at a lower temperature (100 K) and higher density ($\sim 3.0 \times 10^5$ cm^{-3}). The temperature estimated for the extended component agree reasonably well with other determinations from NH_3 and CH_3CN (Tafalla & Bachiller 1995; Codella et al. 2009).

With the physical conditions derived from the CO analysis, we modelled the integrated intensity and the line profile of the o-H_2O $1_{10} - 1_{01}$ transition as well as the reported PACS-measured 179 μm H_2O line intensity ($\sim 10^{-19}$W cm^{-2}, Nisini et al. 2010) to compute the total ortho water abundance in each velocity component. We used a radiative transfer code in the large-velocity gradient approach (and slab geometry) detailed in Melnick et al. (2008), taking into account an ortho to para ratio (OPR) of 1.2 for H_2, as derived from *Spitzer* (Neufeld et al., 2009). Here, we assume the absorption component at +2.9 km is due to foreground gas unrelated to L1157-B1. Together, the two components of the o-H_2O $1_{10} - 1_{01}$ line produce a total H_2O $2_{12} - 1_{01}$ 179 μm line flux of 1.1×10^{-19}W cm^{-2}. For the temperature range derived from our CO analysis, we estimated ortho-H_2O column densities of $(4.0-5.0)\times10^{14}$ cm^{-2} and $(2.5 - 3.0) \times 10^{16}$ cm^{-2} for the LVC and the HVC, respectively. Assuming an OPR of 3, we derived the H_2O abundance from comparison with the gas column densities estimated from CO (see Table 1). We obtained an abundance ratio [H_2O]/[CO] $\simeq$ 0.8 in the high-velocity gas, which is consistent with previous results from ODIN (Benedettini et al. 2002) and agrees reasonably well with the predictions of steady-state C-shock models for this set of physical parameters (shock velocity $V_s \simeq 20$ km s^{-1}, pre-shock density $n(H_2) = 5\times10^3$ cm^{-3}; Gusdorf et al. 2008a,b).

An interesting prediction of our model is that the HVC contribution to the 179 μm flux dominates over the LVC contribution (see last column in Table 1). The higher temperature of this component drives the neutral-neutral reactions that efficiently form H_2O, and the higher shock velocity can more efficiently remove water from grain mantles (see Melnick et al. 2008), resulting in the much greater ortho-H_2O column density than in the LVC. Comparison with NH_3 also suggests that the water production in the HVC is strongly dominated by high-temperature reactions (see Codella et al.). The higher ortho-H_2O column density is what produces the higher 179 μm line flux from this component. Consistent results are obtained by Nisini et al. (2010) based on a 179 μm PACS map and previous ODIN and SWAS observations of the o-H_2O $1_{10} - 1_{01}$ line, assuming one single physical component dominates the water line emission in the HIFI beam. Follow-up observations of the higher-excitation lines of CO and H_2O with HIFI will help us constrain more accurately the physical conditions of each velocity component (density, temperature) and more generally in the shock.

Acknowledgements. HIFI has been designed and built by a consortium of institutes and university departments from across Europe, Canada and the United States under the leadership of SRON Netherlands Institute for Space Research, Groningen, The Netherlands and with major contributions from Germany, France and the US. Consortium members are: Canada: CSA, U.Waterloo; France: CESR, LAB, LERMA, IRAM; Germany: KOSMA, MPIfR, MPS; Ireland, NUI Maynooth; Italy: ASI, IFSI-INAF, Osservatorio Astrofisico di Arcetri- INAF; Netherlands: SRON, TUD; Poland: CAMK, CBK; Spain: Observatorio Astronómico Nacional (IGN), Centro de Astrobiología (CSIC-INTA). Sweden: Chalmers University of Technology - MC2, RSS & GARD; Onsala Space Observatory; Swedish National Space Board, Stockholm University - Stockholm Observatory; Switzerland: ETH Zurich, FHNW; USA: Caltech, JPL, NHSC. HIPE is a joint development by the *Herschel* Science Ground Segment Consortium, consisting of ESA, the NASA *Herschel* Science Center, and the HIFI, PACS and SPIRE consortia.

References

Bachiller, R., Perez-Gutierrez, M., 1997, ApJ, 487, L93

Bachiller, R., Perez-Gutierrez, M., Kumar, M.S.N., Tafalla, M., 2001, A&A, 372, 899
Benedettini, M., Visit, S., Giannini, T., et al., 2002, A&A, 395, 657
Benedettini, M., Viti, S., Codella, C., et al., 2007, MNRAS, 381, 1127
Bergin, E.A., Neufeld, D.A., Melnick, G.J., 1998, ApJ, 499, 777
Codella, C., Benedettini, M., Beltrán, M., et al., 2009, A&A, 507, L25
Codella, C., et al., 2010, this volume
de Graauw, T., et al. 2010, this volume
Elitzur, M., de Jong, T., 1978, A&A, 67, 323
Elitzur, M., Watson, W.D., ApJ, 70 443
Flower, D.R., 2001, J. Phys. B, 34, 2731
Flower, D.R., Pineau des Forets, G., 2010, MNRAS, submitted
Gueth, F., Guilloteau, S., Bachiller, R., 1996, A&A, 307, 891
Gueth, F., Guilloteau, S., Bachiller, R., 1998, A&A, 333, 287
Gusdorf, A., Cabrit, S., Flower, D.R., et al., 2008a, A&A, 482, 809
Gusdorf, A., Pineau des Forets, G., Cabrit, S., et al., 2008b, A&A, 490, 695
Kaufman, M., Neufeld, D., 1996, ApJ, 456, 611
Looney, L.W., Tobin, J.J., Kwon, W., 2007, ApJ, 670, L131
Melnick, G.J., Tolls, V., Neufeld, D.A., et al., 2008, ApJ, 683, 876
Neufeld, D.A., Giannini, T., Melnick, G.J., et al., 2009, ApJ, 706, 170
Nisini, B.,et al., 2010, this volume
Ott, S., 2009, in ASP Conference Series, Astronomical Data Analysis Software and Systems XIX, Y. Mizumoto, K.-I. Morita, and M. Ohishi, eds., in press
Pilbratt, G., et al., 2010, A&A, this volume
Viotti, N.R., 1969, Mem. Soc. Astron. Ital., 40, 75

---

[1] Laboratoire d'Astrophysique de Grenoble, UMR 5571-CNRS, Université Joseph Fourier, Grenoble: e-mail: lefloch@obs.ujf-grenoble.fr
[2] Observatoire de Paris-Meudon, LERMA UMR CNRS 8112. Meudon, France
[3] INAF, Osservatorio Astrofisico di Arcetri, Firenze, Italy
[4] Center for Astrophysics, Cambridge MA, USA
[5] Centro de Astrobiología, CSIC-INTA, Madrid, Spain
[6] CESR, Université Toulouse 3 and CNRS, Toulouse, France
[7] INAF, Istituto di Fisica dello Spazio Interplanetario, Roma, Italy
[8] Infared Processing and Analysis Center, Caltech, Pasadena, USA
[9] School of Physics and Astronomy, University of Leeds, Leeds, UK
[10] Institut de Radio Astronomie Millimétrique, Grenoble, France
[11] Johns Hopkins University, Baltimore MD, USA
[12] INAF, Osservatorio Astronomico di Roma, Monte Porzio Catone, Italy
[13] Max-Planck-Institut für Radioastronomie, Bonn, Germany
[14] Department of Physics and Astronomy, University College London, London, UK
[15] Université de Bordeaux, Laboratoire d'Astrophysique de Bordeaux, France; CNRS/INSU, Floirac, France
[16] California Institute of Technology, Pasadena, USA
[17] University of Michigan, Ann Arbor, USA
[18] Astronomical Institute 'Anton Pannekoek', University of Amsterdam, Amsterdam, The Netherlands
[19] Kapteyn Astronomical Institute, University of Groningen, Groningen, The Netherlands
[20] IGN Observatorio Astronómico Nacional, Spain
[21] Jet Propulsion Laboratory, Caltech, Pasadena, CA 91109, USA
[22] SRON, Groningen, The Netherlands
[23] Max Planck Institut für Astronomie , Heidelberg - Germany
[24] Ohio State University, Columbus, OH, USA
[25] Physikalisches Institut, Universität zu Köln, Köln, Germany
[26] Leiden Observatory, Leiden University, Leiden, The Netherlands
[27] IRAM, Granada, Spain
[28] Department of Astronomy, Stockholm University, Stockholm, Sweden
[29] Radboud University Nijmegen, The Netherlands
[30] Northrop Grumman Aerospace Systems, Redondo Beach, CA 90278 U.S.A